

A Torque Ripple Compensation Technique for a Low Cost Brushless DC Motor Drive

H. K. Samitha Ransara and Udaya K. Madawala, *Senior Member, IEEE*.

Abstract— This paper presents a torque ripple compensation technique for a Brushless DC (BLDC) motor drive that is operated without a DC link capacitor. The motor drive, which uses a single switch control strategy, resembles that of a buck converter during operation at any switching state. A simple buck converter based model is therefore proposed to predict the behaviour of the BLDC motor drive at constant speed. Using the model, the impact of operation without the DC link capacitor on the torque produced by the BLDC motor drive is investigated in detail. Theoretical behaviour of the BLDC motor drive is compared with Matlab/Simulink based simulations to demonstrate the validity of the compensation technique and the analysis. Experimental results of a 250 W prototype motor drive are also presented to further validate the theoretical analysis as well as the effectiveness of the proposed technique. Results convincingly indicate that the BLDC motor drive with torque ripple compensation offers comparable performance.

Index Terms—Brushless machines, Torque ripple compensation

I. INTRODUCTION

PERMANENT Magnet Synchronous (PMS) motors and Brushless DC (BLDC) motors are becoming popular in industrial applications and home appliances. These motors offer many advantages such as high reliability, low maintenance, high efficiency and long operating life in comparison to the other motor types such as induction and brushed DC motors. Both BLDC and PMS motors are electronically commutated using rotor position information, which is obtained by position sensors or estimated using parameters of the motor drive. Consequent up on the recent advances in rare earth magnetic materials, BLDC and PMS motors are now designed with high power densities, making them an attractive choice for space and weight critical applications such as airspace applications and mobile coolers [1].

PMS motors demand continuous rotor position information for their operation. Therefore, continuous angular position sensors or continuous rotor position estimation techniques are required for PMS motors. Moreover, a significant amount of computational time is required to process the vector operations

Manuscript received June 16, 2014; revised October 6, 2014 and December 28, 2014; accepted January 18, 2015.

Copyright © 2015 IEEE. Personal use of this material is permitted. However, permission to use this material for any other purposes must be obtained from the IEEE by sending a request to pubs-permissions@ieee.org.

H. K. Samitha Ransara and Udaya K. Madawala are with The University of Auckland, Auckland, 1020, New Zealand (e-mail: shew023@aucklanduni.ac.nz).

which are needed to control the motor effectively.

In contrast, three-phase BLDC motors only require rotor position information for every 60 electrical degrees, which can be derived from three inexpensive Hall effect sensors or a back emf sensing technique. Therefore, BLDC motors have become the preferred choice for industry applications where efficient, compact and cost effective motor drives are required [1]-[3].

A typical BLDC motor drive with rotor position feedback is illustrated in Fig. 1(a). The motor drive comprises a diode rectifier, a large electrolytic capacitor and a converter fed with rotor position information. The electrolytic capacitor is bulkier in size and weight, and its lifetime is severely affected by the operating temperature [4]. Thus, the inclusion of the capacitor reduces the reliability of the motor drive, particularly in hot or cold environments such as in heating, ventilation and air conditioning applications. Moreover, electrolytic capacitor technology is relatively stable, and the price is governed only by the cost of materials. Therefore, the cost of an electrolytic capacitor is more or less static compared to costs associated

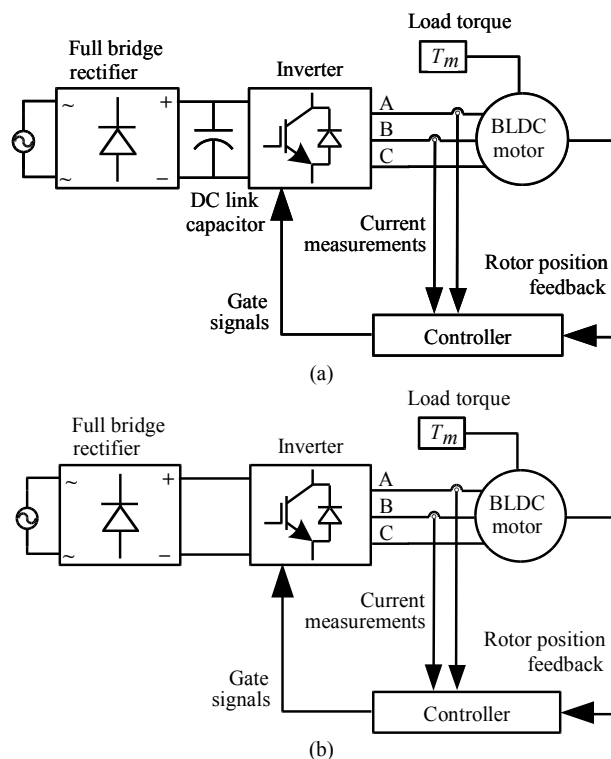


Fig. 1. (a) A typical BLDC motor drive; and (b) a BLDC motor drive without a DC link capacitor.

with processors, power electronic switches and driver circuits. For example, the cost of the DC link capacitor is approximately 5% – 15% of the overall cost of BLDC motor drives made by Wellington Drive Technologies Ltd. In addition, the absence of the DC link capacitor yields a reduction of 4% – 15% in the area of the printed circuit board and the volume of the enclosure. Thus, to reduce the cost of components, minimize the size of the enclosure and to increase the reliability, a BLDC motor drive without a DC link capacitor is proposed in [5] and illustrated in Fig. 1(b).

Without the DC link capacitor, the motor drive is operated directly from a rectified mains supply. The cost of the overall motor drive is significantly reduced due to the absence of the DC link capacitor but at the expense of torque ripples, which are inevitable and expected to be around zero crossings of the mains supply. Various techniques have been proposed and successfully implemented to compensate for the torque ripples in BLDC motor drives that are caused by current commutation between phases and cogging. These compensation techniques can be broadly classified into two mainstreams. The first mainstream is physical modifications of the motor to reduce the torque ripple. Techniques such as altering the magnetic design of stator and rotor [6]-[7] and altering the windings [8] to compensate for the pulsating torque have been reported in literature. The second mainstream is modifications of the controller to compensate for the torque ripple. This includes the techniques such as adaptive torque control [9]-[10], current shaping techniques [11]-[12], controlling the input voltage to reduce the torque ripple [13], implementing a feed forward current controller [14] and direct torque control [15]-[16]. Compensating for the torque ripple due to asymmetric motor parameters by using an online estimation technique has been reported in [17]. A real time duty cycle modulation technique to reduce the torque ripple that is caused by non-ideal back emf in practical BLDC motor drives has been reported in [18]. A technique to reduce the torque ripple by estimating the torque and compensating with a feed forward current control technique has been reported in [19] for BLDC motors with low inductance. An accelerated torque control technique that utilizes a disturbance torque observer has been reported in [20]. Switching capacitors have been used in matrix converter based systems previously and proved to be a success. For example, actively controlled and switched capacitors on the DC link to compensate for the inherent torque ripples in BLDC motors that are driven by matrix converters have been proposed and validated by experiments in [21]-[22]. With the technological advancements, compensation of torque ripples through modifying the controller and control algorithm gains popularity in contrast to altering physical structure of the BLDC motor. Nevertheless, no attempts have been reported to compensate for the torque ripple associated with the DC link capacitor free BLDC motor drives.

This paper therefore presents a technique to compensate for the torque ripple of a low cost BLDC motor that is driven without a DC link capacitor. The proposed compensation technique utilizes a small capacitor on the DC link to energize the motor on demand. The small compensation capacitor is

typically around 3% of the original DC link capacitance. Benefits of employing such a small capacitor on the DC link with the switch outweigh the disadvantages caused by the absence of the DC link capacitor. A simple buck converter based mathematical model is presented to accurately predict the torque produced by the BLDC motor drive at constant speed [23]. The computational complexity of the proposed buck model is considerably lower compared to the comprehensive model of the BLDC motor drive without a DC link capacitor that is reported in [24]. Both speed and torque of the motor are regulated by using a six step switching pattern but controlling only one of the two switches at a given moment. The buck model is used for the selection of the controlled capacitor that is used for compensating the torque ripple. Theoretical analysis of the proposed simple buck model of the BLDC motor drive is validated by using Matlab/Simulink simulations and experimental results. In addition, results produced by the comprehensive buck model [24] and the simple buck model [23] are compared to evaluate the accuracy of the simple buck model. Also, a cost comparison between a conventional BLDC motor drive and the proposed motor drive is included in this paper. With the proposed compensation technique, torque ripples caused by the absence of the bulkier DC link capacitor are fully eliminated. Results convincingly indicate that the proposed compensation technique is effective, inexpensive and can be used in design of practical BLDC motor drives.

II. MATHEMATICAL MODEL

In three-phase BLDC motor drives with trapezoidal back emf, only two phases are energized based on the rotor position information at any given instant in time. Switches that are connected to the third phase remain in off state. As such, only two switches of the inverter are in conduction at any particular instant. Usually, these two switches are controlled using PWM or hysteric control signals generated from a microcontroller, either in torque control or speed control mode. However, such a switching strategy is not appropriate for motor drives with no DC link capacitor since there is no continuation path for the phase current during off state of the two controlled switches. In the proposed BLDC motor drive, a switching algorithm, which is based on single switch control while keeping the other switch in on state for the entire switching interval, is employed. The switch that remains in on state provides a

TABLE I
SWITCHING ALGORITHM

| Step | Hall sensor output | | | Switch is in on state | Controlled switch |
|------|--------------------|-------|-------|-----------------------|-------------------|
| | H_a | H_b | H_c | | |
| 1 | 1 | 0 | 0 | A_1 | C_2 |
| 2 | 1 | 1 | 0 | C_2 | B_1 |
| 3 | 0 | 1 | 0 | B_1 | A_2 |
| 4 | 0 | 1 | 1 | A_2 | C_1 |
| 5 | 0 | 0 | 1 | C_1 | B_2 |
| 6 | 1 | 0 | 1 | B_2 | A_1 |

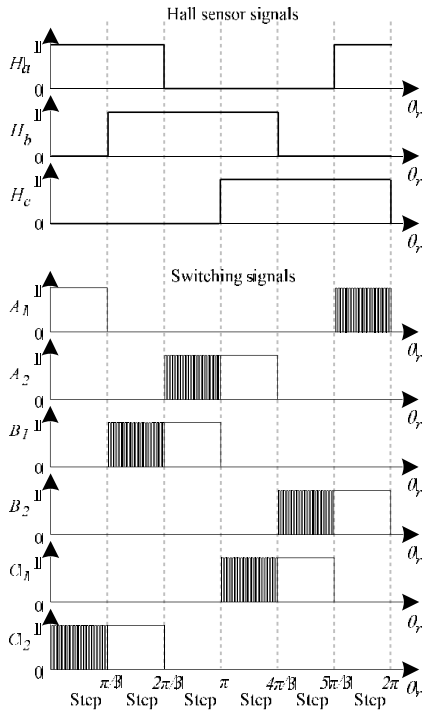


Fig. 2. Hall sensor signals and switching signals.

freewheeling path to the inductive current while the controlled switch in off state. The switching states are tabulated in Table I with rotor position information obtained by Hall effect sensors. The outputs of Hall effect sensors, denoted by H_a , H_b and H_c , and switching signals are illustrated in Fig. 2 with the position of the rotor, denoted by θ_r , in electrical radians. Switches of the phase legs A, B, and C of the inverter are represented by A_1 , A_2 , B_1 , B_2 , C_1 and C_2 where subscripts 1 and 2 denote the upper and the lower switch of each phase leg of the inverter, respectively.

Consider the operation of the motor drive in step 2 of the switching algorithm during which switch B_1 is controlled while switch C_2 is left on. Phase A remains in off state. Fig. 3(a) and Fig. 3(b) illustrate the current paths when the switch B_1 is on and off, respectively. As evident from Fig. 3, the operation of the motor drive during step 2 is similar to that of a buck converter and can be represented by a model shown in Fig. 4. The operation of the motor drive during all other steps of the switching algorithm can be represented by the same buck converter model. Since two phases are lumped together, $e(t)$ represents the line-to-line back emf (V), and S and D in Fig. 4 represent the controlled switch and freewheeling diode, respectively.

From Fig. 3, the BLDC motor drive during on and off states of switch S can be expressed by,

$$v_{in}(t) = 2i_m(t)R + 2(L-M)\frac{di_m(t)}{dt} + e(t) \quad (1)$$

$$0 = 2i_m(t)R + 2(L-M)\frac{di_m(t)}{dt} + e(t) \quad (2)$$

where v_{in} is the input voltage to the buck converter (V), i_m is the phase current (A), R is the resistance of a phase winding (Ω), L is the inductance of a phase winding (H) and M is the mutual inductance between phase windings (H), respectively.

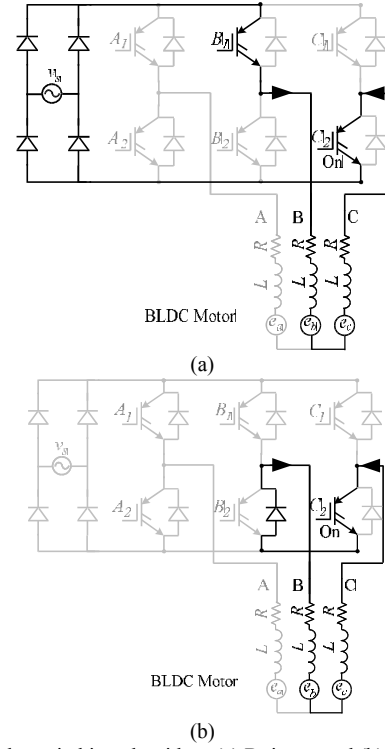


Fig. 3. Step 2 of the switching algorithm: (a) B_1 is on; and (b) B_1 is off.

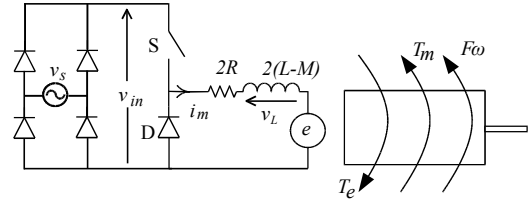


Fig. 4. A buck converter based model of the motor drive.

If R is assumed to be small, (1) and (2) can be simplified to,

$$v_{in}(t) = 2(L-M)\frac{di_m(t)}{dt} + e(t) \quad (3)$$

$$0 = 2(L-M)\frac{di_m(t)}{dt} + e(t) \quad (4)$$

The assumption of neglecting R is numerically validated in the results section for the parameters of the motors that are used in this study.

Let ω be the speed of the rotor in rads^{-1} . Then the torque produced by the motor, denoted by T_e (Nm), can be given as,

$$T_e = \frac{e(t)i_m(t)}{\omega} \quad (5)$$

The equation of motion of the motor drive can be given as,

$$T_e - T_m = J\frac{d\omega(t)}{dt} + F\omega(t) \quad (6)$$

where J is the combined inertia (kgm^2) of the rotor and load and F is the mechanical viscous friction coefficient (Nm/s).

Electrical and mechanical speed of the motor are related by,

$$P\omega = \frac{d\theta_r}{dt} \quad (7)$$

where P is the number of pole pairs of the BLDC motor.

Generally, the back emf waveform is trapezoidal for BLDC motor drives. However, in practice, the ideal trapezoidal back emf waveform can be slightly distorted by harmonics. To simplify the analysis, a BLDC motor with

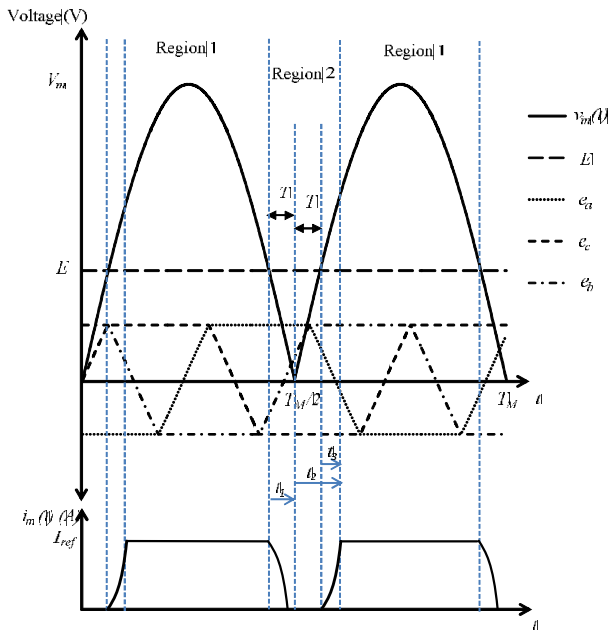


Fig. 5. Controllable and uncontrollable regions of current of the motor drive at steady state.

ideal trapezoidal back emf is assumed. Two of the motor phases are energized during the constant 120° region of the trapezoidal back emf waveform and the magnitude of $e(t)$ during this time is defined as E . If there are significant deviations in the actual back emf waveforms with the ideal trapezoidal shape, the average value of the actual back emf during the 120° period can be used as E to simplify the model and analysis. Nevertheless, higher order harmonics of the generated back emf can also be taken into consideration at the expense of additional computational complexity. In this particular drive as well as for most BLDC drives, the energy loss associated with commutation is low and, hence, the effect of commutation is neglected to further simplify analysis.

The motor drive is fed by the input voltage v_{in} that varies between 0-325 V due to the absence of the DC link capacitor. As such, build-up of phase current, which is given by (3) and dictated by the back emf and inductance, is possible only during one region of the rectified mains voltage and when the voltage across inductance, denoted as v_L , is positive. Fig. 5 illustrates the rectified mains supply voltage for a given reference current and is divided into region 1 and region 2 based on whether or not the phase current can be maintained at the reference value. A typical motor phase current waveform is also illustrated.

As evident from (3) and (4), the phase current is non-linear and uncontrollable during region 2. Consequently, the torque will also be uncontrollable in region 2. In addition, the duration of region 2 is governed by the value of back emf and increases with high back emf. Therefore, it is important to investigate the impact on the developed torque due to uncontrollable current region in comparison to a typical BLDC motor drive.

The duty cycle of the switch, defined as $D(t)$, is time varying over a half cycle of $v_{in}(t)$. Due to lower input voltage in region 2 compared to the back emf, the controller operates the switch at the maximum possible duty cycle of 100%.

Times T and T_M are defined as the interval for $v_{in}(t)$ to reach E from 0V and the period of the input mains voltage, respectively.

As such, T can be given as,

$$T = \frac{1}{2\pi f} \sin^{-1} \left(\frac{E}{V_m} \right) \quad (8)$$

where, V_m and f are the peak value (V) and the frequency (Hz) of the input supply voltage, respectively.

Current $i_m(t)$ is derived as a piecewise function of time during region 2. Consequently, the generated torque by the motor can also be represented as a piecewise function. The following variables in time are defined to express $i_m(t)$ as a piecewise function, and, thus, to reduce the complexity in expressions.

$$t_1 = t - \left(\frac{T_m - T}{2} \right) \quad (9)$$

$$t_2 = t - \left(\frac{T_m}{2} \right) \quad (10)$$

$$t_3 = t - \left(\frac{T_m + T}{2} \right) \quad (11)$$

For example, $i_m(t_1)$ and $v_L(t_1)$ represent the phase current and the voltage across the inductance in region 2 when $(T_m/2 - T) \leq t \leq T_m/2$, respectively. The input voltage to the motor $v_{in}(t)$ is assumed as a piecewise linear function during region 2 to simplify the analysis.

From Fig. 5, $v_L(t_1)$ can be approximated as follows.

$$v_L(t_1) = -\frac{E}{T} t_1 \quad (12)$$

However, $v_L(t)$ can be given as,

$$v_L(t) = 2(L - M) \frac{di_m(t)}{dt} \quad (13)$$

From (12) and (13),

$$2(L - M) \frac{di_m(t_1)}{dt_1} = -\frac{E}{T} t_1 \quad (14)$$

The general time domain solution for (14) can be given as,

$$i_m(t_1) = -\frac{Et_1^2}{4(L - M)T} + C \quad (15)$$

Substitution of the initial condition, which is $i_m = I_{ref}$ at $t_1 = 0$ yields,

$$C = I_{ref} \quad (16)$$

From (15) and (16), the complete time domain solution for $i_m(t_1)$ can be given as follows.

$$i_m(t_1) = -\frac{Et_1^2}{4(L - M)T} + I_{ref} \quad (17)$$

From (17), the necessary and sufficient condition for $i_m(t)$ to be discontinuous before the zero crossing of $v_{in}(t)$ can be mathematically expressed as follows.

$$(L - M) < \frac{ET}{4I_{ref}} \quad (18)$$

From (18) it is evident that, if the equivalent line-to-line inductance is greater than $ET/2I_{ref}$, $i_m(t)$ is continuous at the zero crossing of $v_{in}(t)$. The value of $i_m(t)$ at the zero crossing, defined as I_m , is given by,

$$I'_m = \frac{-ET}{4(L-M)} + I_{ref} \quad (19)$$

From Fig. 5, $v_L(t_2)$ can be approximated as follows.

$$v_L(t_2) = \left(\frac{E}{T}\right)t_2 - E \quad (20)$$

From (20) substituting to $v_L(t_2)$ yields,

$$2(L-M) \frac{di_m(t_2)}{dt_2} = \left(\frac{E}{T}\right)t_2 - E \quad (21)$$

The general time domain solution for (21) can be given as,

$$i_m(t_2) = \frac{Et_2^2}{4(L-M)T} - \frac{Et_2}{2(L-M)} + C \quad (22)$$

Substitution of the initial condition given in (19) in (22) yields,

$$i_m(t_2) = \frac{Et_2^2}{4(L-M)T} - \frac{Et_2}{2(L-M)} - \frac{ET}{4(L-M)} + I_{ref} \quad (23)$$

Equation (23) represents $i_m(t)$ after the zero crossing of $v_{in}(t)$. Moreover, it is possible to derive the necessary and sufficient condition for $i_m(t)$ to be continuous during region 2 by inspecting the sign of (23) at $t_2 = T$.

$$L-M > \frac{ET}{2I_{ref}} \quad (24)$$

Therefore, if the equivalent line-to-line inductance of the motor is less than ET/I_{ref} , $i_m(t)$ is discontinuous during region 2. Then, $i_m(t)$ starts to build-up after $t = T_M/2 + T$.

From Fig. 5, $v_L(t_3)$ can be approximated as follows.

$$v_L(t_3) = \left(\frac{E}{T}\right)t_3 \quad (25)$$

From (25) substituting to $v_L(t_3)$ yields,

$$2(L-M) \frac{di_m(t_3)}{dt_3} = \left(\frac{E}{T}\right)t_3 \quad (26)$$

The general time domain solution for (26) can be given as,

$$i_m(t_3) = \frac{Et_3^2}{4(L-M)T} + C \quad (27)$$

Substituting the initial condition, which is $i_m(t_3) = 0$ at $t_3 = 0$ yields $C = 0$. Hence, the complete solution for $i_m(t_3)$ can be given as follows.

$$i_m(t_3) = \frac{Et_3^2}{4(L-M)T} \quad (28)$$

Equation (28) represents the build-up of $i_m(t)$ as a function of t_3 and is only valid if $i_m(t)$ is discontinuous during region 2.

Equations (17), (23) and (28) can be used to obtain the instantaneous torque during region 2, the average torque produced by the motor drive and the reduction of the average torque at constant speed operation without the DC link capacitor. Moreover, this analysis facilitates a performance comparison between the proposed motor drive and a conventional motor drive under different operating conditions for different motor parameters. Dynamics of the current in region 2 depend on whether the current is discontinuous or not in region 2. Eq. (17) represents $i_m(t)$ until $v_{in}(t)=0$. If $i_m(t)$ is continuous in region 2, (23) represents the dynamics of $i_m(t)$ in region 2 after $v_{in}(t)=0$. If $i_m(t)$ is discontinuous in region 2 after $v_{in}(t)=0$, (23) provides the dynamics of $i_m(t)$ until to the point where $i_m(t)=0$. Then, $i_m(t)$ starts to build-up during t_3 and is governed by (28).

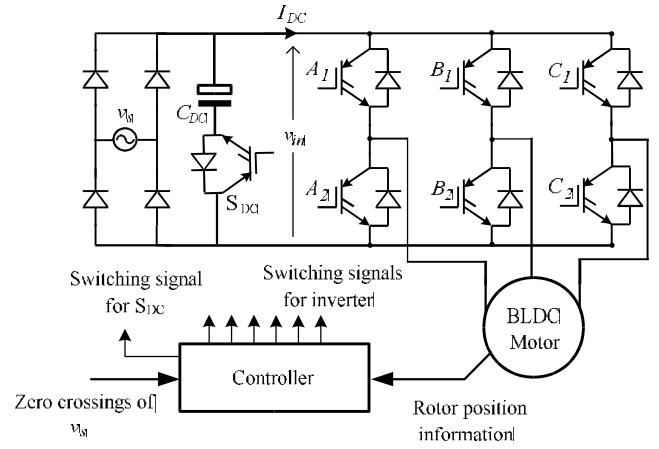


Fig. 6. Proposed technique for torque ripple compensation.

III. COMPENSATING FOR THE TORQUE RIPPLE

The proposed DC link capacitor free BLDC motor drive produces torque ripples and discontinuities in region 2 due to uncontrollable phase current. Such ripples and discontinuities are not preferred in some applications, which require a constant torque output. Moreover, discontinuities in the torque result in vibrations and acoustic noise in the motor drive. Those vibrations can cause undesirable stresses on the mountings and bearings, raising reliability concerns of the motor drive system. In addition, the average torque produced by a motor drive without the DC link capacitor is lower in comparison to a motor drive with stiff DC link. As a solution, a torque ripple compensation technique based on an actively controlled small capacitor is proposed and illustrated in Fig. 6. During region 1 of Fig. 5, C_{DC} is charged through the anti-parallel freewheeling diode associated with S_{DC} . However, there is no natural discharging path for the capacitor, and the discharge can be controlled by the gate signal applied to S_{DC} . The energy stored in C_{DC} should be sufficient to keep $i_m(t)$ at I_{ref} during region 2 to eliminate the torque ripple. The controller is developed in such a way that the gate signal applied to S_{DC} is derived based on E and $v_{in}(t)$, while controlling the other switches in the inverter.

Line-to-line back emf E can be calculated by the speed of the motor, which can be obtained using the rotor position information in accordance with (7). Since C_{DC} only supplies energy to the motor during region 2 when $E > v_{in}(t)$, the size of C_{DC} is smaller compared to a DC link capacitor used in a conventional BLDC motor drive. Thus, an inexpensive capacitor and a switch can be used to compensate for the torque ripple.

The value of C_{DC} is selected in such a way that C_{DC} is able to maintain the DC link voltage during region 2 when $E > v_{in}(t)$ in order to maintain $i_m(t)$ at I_{ref} , and is given by,

$$C_{DC} \frac{dV_{in}(t)}{dt} = I_{avg} \quad (29)$$

where I_{avg} denotes the average current drawn from the DC link to maintain $i_m(t)$ at I_{ref} . The voltage derivative represents the rate of change in voltage across C_{DC} during region 2 when $E > v_{in}(t)$. Deriving an analytical solution for I_{avg} is complicated as the duty cycle of the switch is time varying due to $v_{in}(t)$ and the discrete nature of the current drawn from the DC link. However, I_{avg} can be obtained by the buck converter based

simulation model. If I_{avg} is provided by the DC link throughout region 1 and region 2, ripples in torque are eliminated as there will be no discontinuities in the motor phase current. By approximating the derivative, the minimum value of C_{DC} that is required to provide I_{avg} from the DC link is given by,

$$C_{DC} = \frac{2TI_{avg}}{V_m - E} \quad (30)$$

Although the system is more complex with a switch and a small capacitor, the overall cost of the motor drive is expected to be reduced. Since the control of the switch is simple, additional components that ensure fast switching are not required. Therefore, the difference in cost between a conventional BLDC motor drive and a motor drive with proposed compensation is minimized to the difference between the cost of the DC link capacitor, and the cost of the switch, the small capacitor and the isolated gate driver. A price comparison between the DC link capacitor and additional electronics that is required for proposed compensation is tabulated in Table II. The total cost of the electronics is 29.00 USD for the conventional converter that is used in this study. As evidenced, around 6% of the total cost can be reduced from the Bill of Materials (BOM) by using the proposed torque ripple compensation technique.

Bulkier DC link capacitors are rated for finite amount of hours, in contrast to semiconductor switches. As such, by removing the DC link capacitor, the reliability of the overall motor drive is expected to be improved. The applicability of the motor drive has been decreased due to periodic torque ripples that are inevitable due to the absence of the bulkier DC link capacitor. The compensation capacitor is typically about 3% of the original electrolytic DC link capacitor value. As such, for some applications, ceramic capacitors, which are reliable than the electrolytic capacitors, can be used to compensate for the torque ripple. Also, the motor drive can operate with a torque ripple even if the compensation technique failed. A traditional motor drive cannot operate with a failed DC link capacitor. As such, the reliability of the motor drive has not been affected with the additional components. In theory, the reliability of the proposed motor drive should be higher, as there is no bulkier electrolytic DC link capacitor and the motor drive can be operated even with failed DC link components. The switching loss of the

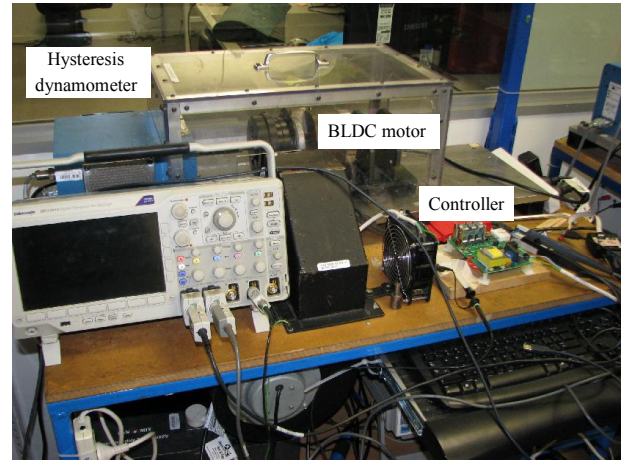


Fig. 7. Experimental setup

additional switch is not dominant due to the lower switching frequency and current in comparison to the IGBTs in the inverter. The obtained efficiency figures by experiments, that are included in the paper with and without the proposed compensation technique and the estimated switching loss values, suggest that the switching loss of the additional switch is not dominant. With the absence of the bulkier DC link capacitor, an improvement in the Total Harmonic Distortion (THD) of the input current is expected as well.

Due to the small torque ripple compensation capacitance, magnitudes of the capacitor charging currents are low. Therefore, transient problems associated with the proposed compensation technique are low. Measured DC link voltages reported in Section V indicates that the transient problems are minimal with the proposed compensation.

However, with the proposed compensation technique, the overall motor drive becomes more complex, which is a major disadvantage. In terms of hardware components, an additional driving stage and an IGBT are needed. Moreover, the firmware has to be modified to control the additional switch. For some applications, an augmentation in the microcontroller platform might be required to facilitate the torque ripple compensation technique. The cost of the torque ripple compensation technique could be higher than the conventional BLDC motor drive for such scenarios. That will void the cost benefit of the proposed torque ripple compensation technique. Moreover, if this compensation technique needs to be introduced to an existing product, a significant changes in PCB layout and production assembly process are needed, which increase the capital cost of the product.

TABLE II

COST COMPARISON BETWEEN THE CONVENTIONAL CONVERTER AND THE PROPOSED COMPENSATION TECHNIQUE

| | Conventional converter (USD) | Proposed technique (USD) |
|--|------------------------------|--------------------------|
| Electrolytic DC link capacitor 150 μ F/400 V | 3.8 | 0 |
| 4.7 μ F/400 V capacitor | 0 | 0.29 |
| IGBT 600 V / 10 A | 0 | 0.51 |
| Isolated gate driver 5.3 kVrms /2.5 A | 0 | 1.12 |
| Sub total | 3.8 | 1.92 |
| Saving due to compensation | N/A | 1.88 |
| Percentage saving from the total BOM cost | N/A | 6% |

IV. IMPLEMENTATION

To validate the proposed model and analysis, a prototype BLDC motor controller was implemented. Two BLDC motors, which are manufactured by Wellington Drive Technologies with different motor parameters, were used to obtain the experimental results. The parameters of the two motors, named as M1 and M2, are tabulated in Appendix. Hall effect sensors mounted in the motor were used to derive the gate signals according to the proposed switching algorithm by using a microcontroller. The simplicity of the derived model permits the implementation of the controller in an

inexpensive microcontroller platform. As such, cost of the controller can be reduced, which is an advantage of the proposed technique. Experiments were performed with a current reference of 1 A. Controlled load torque values are applied to the drive by using a hysteresis dynamometer to obtain different operating conditions. The experimental setup is shown in Fig. 7.

V. RESULTS

The mathematical expressions derived for $i_m(t)$ are numerically solved for different motor parameters to evaluate the average value and continuity of $i_m(t)$. To investigate the accuracy, the theoretical results obtained from the mathematical model are compared with Matlab/Simulink simulations and experimental results. Moreover, the results are compared with the results obtained for a conventional BLDC motor drive with a stiff DC link.

According to the expressions derived, three test cases can be identified based on the continuity of $i_m(t)$ during region 2.

1. Case 1 - $i_m(t)$ is discontinuous before the zero crossing of $v_{in}(t)$.
2. Case 2 - $i_m(t)$ is continuous.
3. Case 3 - $i_m(t)$ is discontinuous after the zero crossing

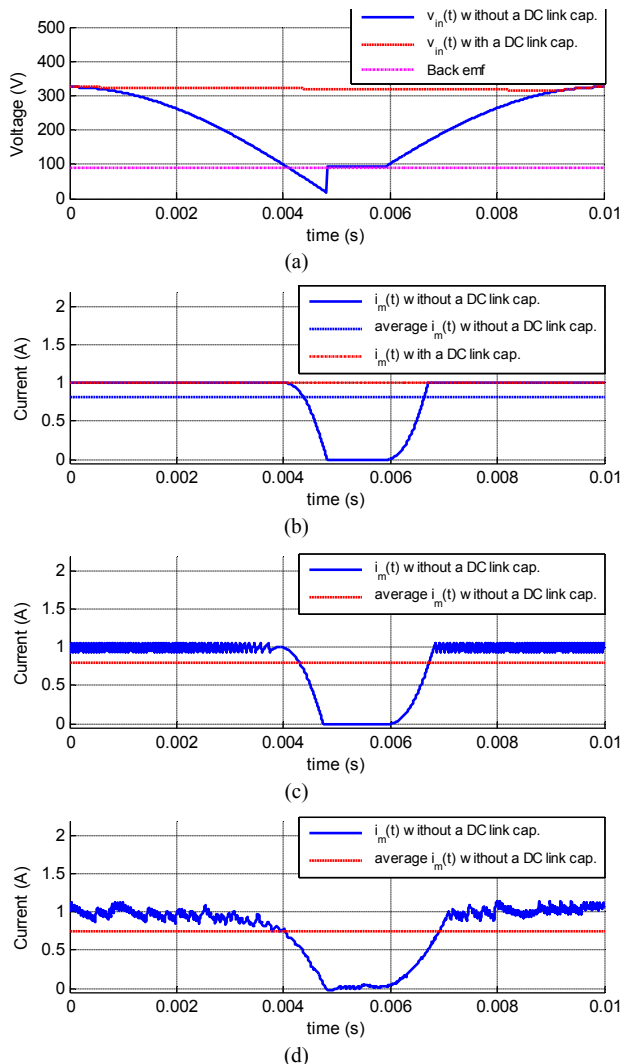


Fig. 8. Case 1 with M1 for $E = 95V$: (a) $v_{in}(t)$ and E ; (b) $i_m(t)$ by theoretical analysis; (c) $i_m(t)$ by simulation; and (d) $i_m(t)$ by experiment.

of $v_{in}(t)$

Fig. 8 illustrates the theoretical results obtained for the case 1 with M1 and a comparison with Simulink and experimental results. In region 2, the initial decrement of the phase current until the point where it is discontinuous is given by (17). The build-up of the phase current until I_{ref} is given by (28). As evident from the obtained results for this test case, the phase current is discontinuous for a longer time interval. Consequently, the period where there is no output torque is large. As a result, the produced torque has higher distortion and the value of the average torque is low.

Fig. 9 illustrates the theoretical results obtained for the case 2 with M2 and a comparison with Simulink and experimental results. During region 2, the phase current is given by (17) until the zero crossing of input voltage and after that the phase current is given by (23). The average torque produced by the motor is larger in this case as the value of the average phase current is higher. In addition, the distortion in the torque is lower compared to test case 1.

Fig. 10 illustrates the theoretical results obtained for the case 3 with M1 and a comparison with Simulink and experimental results. The phase current until the zero crossing of input voltage is given by (17), and then the phase current is

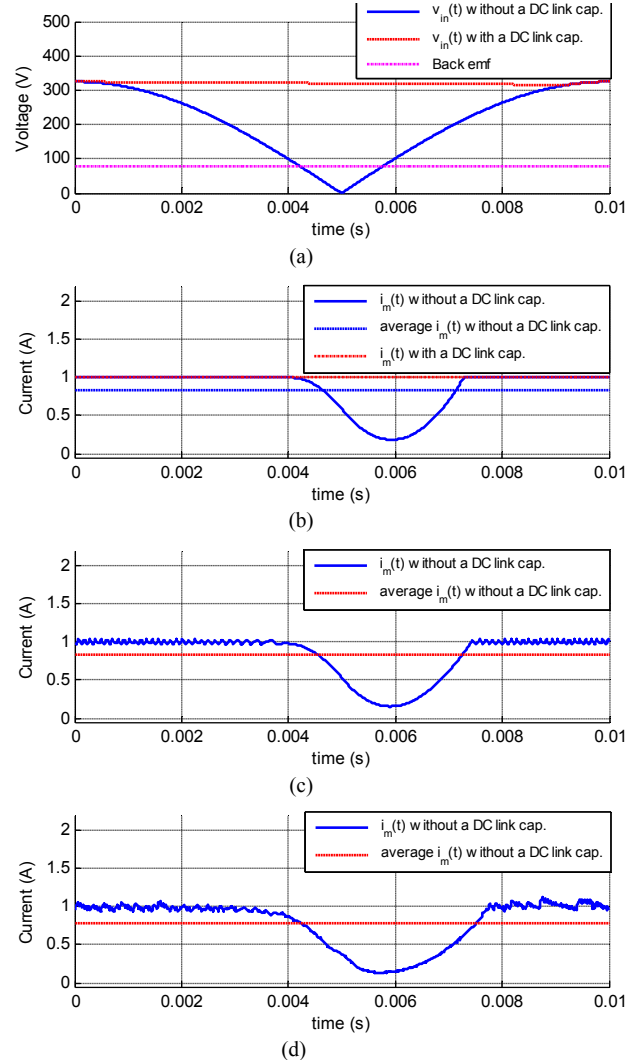


Fig. 9. Case 2 with M2 for $E = 80V$: (a) $v_{in}(t)$ and E ; (b) $i_m(t)$ by theoretical analysis; (c) $i_m(t)$ by simulation; and (d) $i_m(t)$ by experiment.

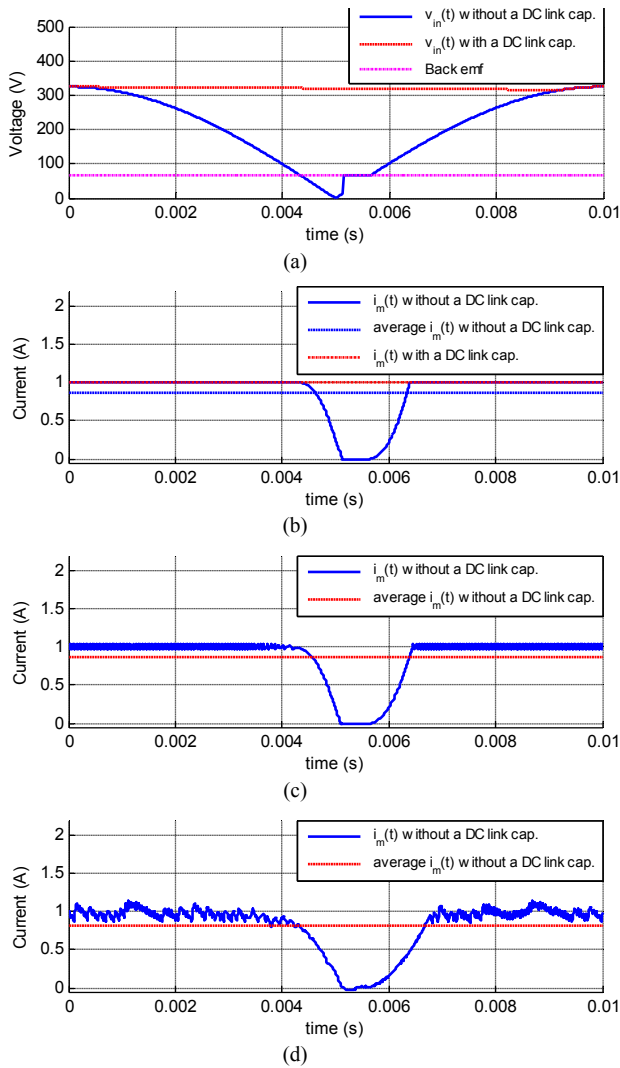


Fig. 10. Case 3 with M1 for $E = 65$ V: (a) $v_{in}(t)$ and E ; (b) $i_m(t)$ by theoretical analysis; (c) $i_m(t)$ by simulation; and (d) $i_m(t)$ by experiment.

given by (23) until the point where it is discontinuous. The build-up of phase current until I_{ref} is given by (28). The time interval where there is no output torque is smaller in this case compared to the first test case. Consequently, the average torque produced by the motor is higher compared to the first test case.

Fig. 11 illustrates a comparison between the results obtained by the comprehensive model with R that is reported in [24] and the simplified model without R that is used in this paper. As evident from Fig. 11, the assumption of neglecting R to simplify the model is verified for the parameters of the motors that are considered in this study. Since R of M2 is higher than that of M1, a slight deviation in the calculated phase currents between the comprehensive model and the simple model is evident in case 2.

Fig. 12 illustrates the current drawn from the DC link for case 1. The boundaries of region 1 and T are marked in the figure. From (8), T for case 1 can be calculated as follows.

$$T = \frac{\sin^{-1}(95/325)}{2 \times \pi \times 50} = 0.94 \text{ ms}$$

The average current drawn from the DC link can be found using numerical methods from Fig. 12. According to the

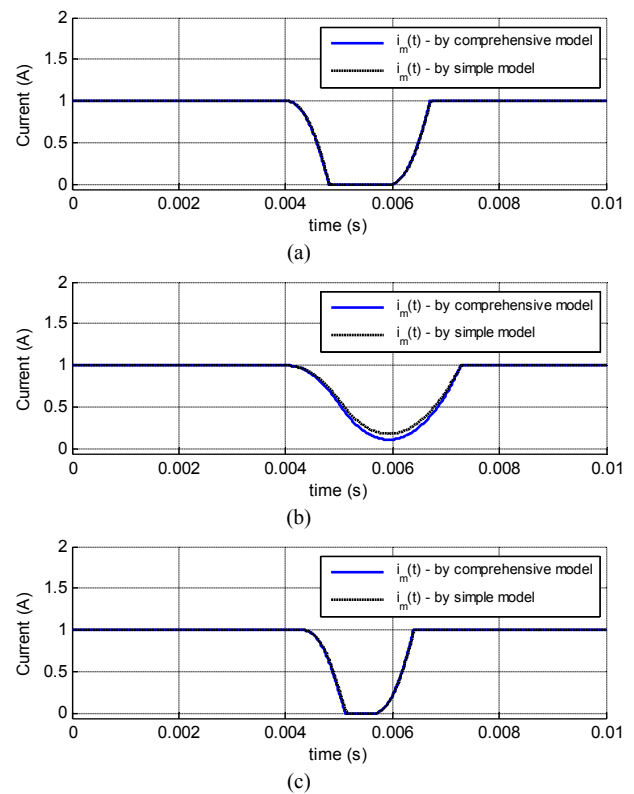


Fig. 11. A comparison between the comprehensive model and the simple model: (a) case 1 with M1; (b) case 2 with M2; and (c) case 3 with M1.

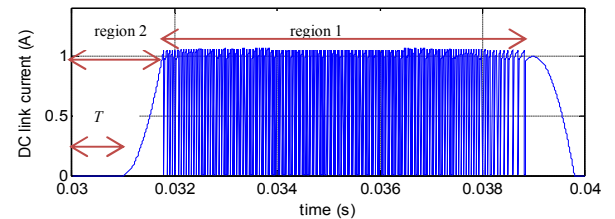


Fig. 12. Current drawn from the DC link for Case 1

numerical solution, I_{avg} equals to 0.44 A. If the compensation capacitor can provide this current during the time when $E > v_{in}(t)$ in region 2, the torque ripple is eliminated. According to Fig 5, the total duration where $E > v_{in}(t)$ equals to $2T$. By substituting the values in (30), minimum C_{DC} is calculated to be equal to 3.61 μF for case 1. So in practice 4.7 μF capacitor can be used as a compensation capacitor. The cost difference between such small capacitors is insignificant in comparison to bulkier DC link capacitors that are normally in use.

Fig. 13(a) and Fig. 13(b) provide a comparison of the phase current without a DC link capacitor, with a DC link capacitor and with the proposed compensation. Fig. 13(c) illustrates the experimental results with the proposed compensation. Fig. 13(d) illustrates the measured DC link voltage. As evident from Fig. 13, the motor current with the proposed compensation is similar to that of a conventional BLDC motor drive with a large DC link capacitor. Also, the compensation technique maintains $v_{in}(t) > E$. As such, according to the derived detailed buck converter based model, the torque ripples in the motor drive without the DC link capacitor are eliminated. The average current drawn from the DC link for case 3, which corresponds to a different load point, can also be

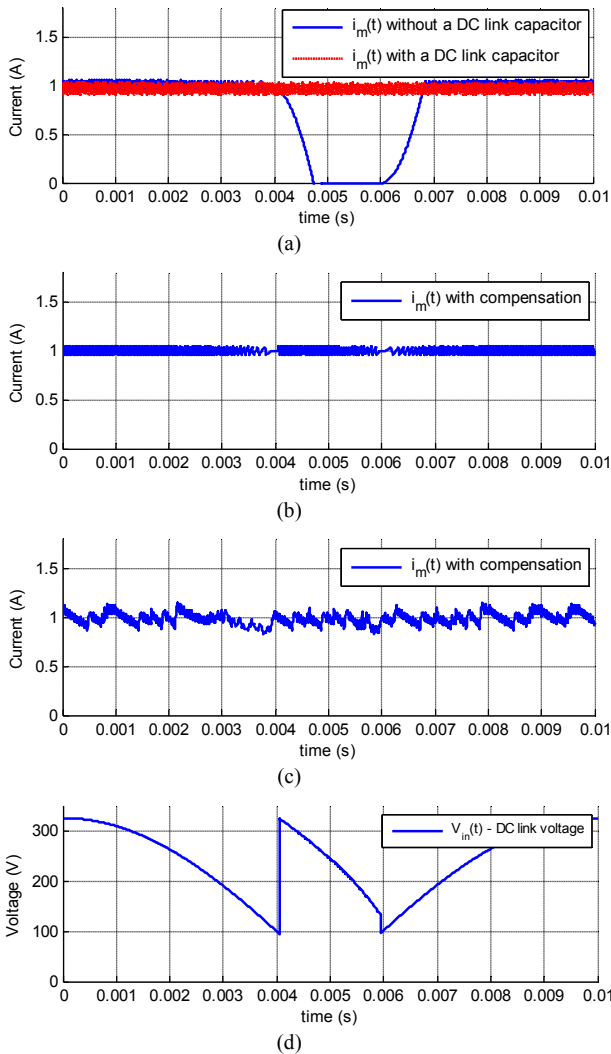


Fig. 13. Proposed compensation for case 1: (a) simulated $i_m(t)$ without a capacitor and with a 150 μF capacitor; (b) simulated $i_m(t)$ with proposed compensation; (c) experimental $i_m(t)$; and (d) DC link voltage with proposed compensation.

calculated through the simulation model. According to the numerical solution I_{avg} for case 3 equals to 0.33 A. The time value T corresponds to case 3, from (8), is 0.64 ms. According to (30), a capacitance of 1.62 μF is sufficient as a compensation capacitor. Since the compensation capacitance used calculated for case 1 is higher than that of case 3, the same compensation circuit can be used throughout the range of load points considered in this paper. Fig. 14(a) and Fig. 14(b) provide a comparison of the phase current without a DC link capacitor, with a DC link capacitor and with the proposed compensation for case 3. Fig. 14(c) illustrates the experimental results with the proposed compensation for case 3. Fig. 14(d) illustrates the measured DC link voltage with the proposed compensation.

To estimate the loss introduced by the additional IGBT, which is used in the compensation circuit, the current through the IGBT is measured. The current through the IGBT is highest for case 1, and measured to be equal to 0.35A. On state resistance of the IGBT (R_{ON}) is obtained using the output characteristics. From the datasheet, for $V_{GE} = 15\text{V}$, R_{ON} is approximated to be equal to 0.08 Ω . Conduction loss (P_c) can be found by,

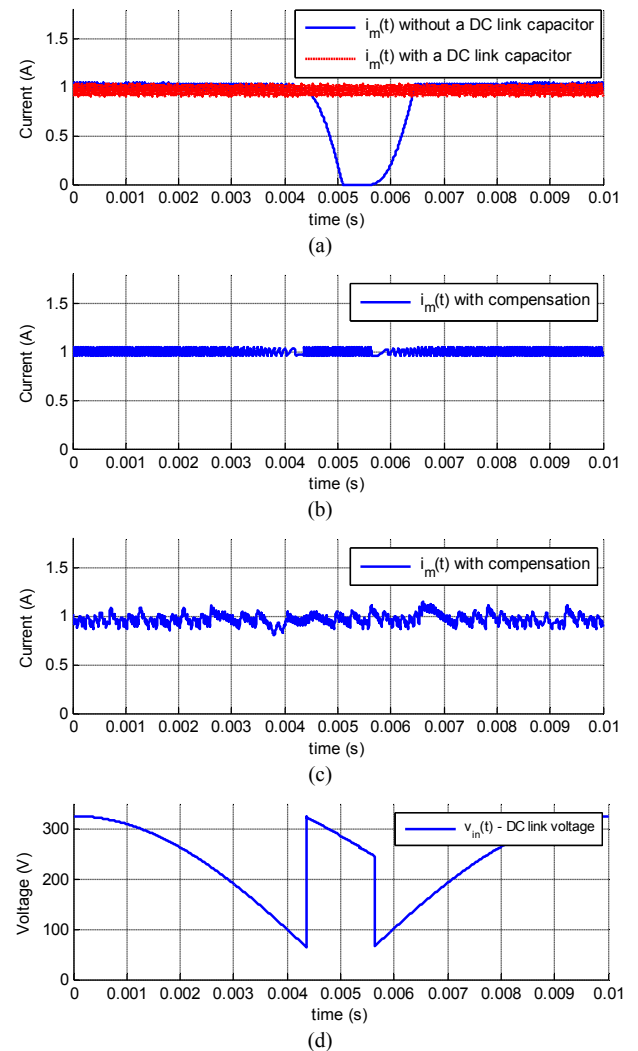


Fig. 14. Proposed compensation for case 3: (a) simulated $i_m(t)$ without a capacitor and with a 150 μF capacitor; (b) simulated $i_m(t)$ with proposed compensation; (c) experimental $i_m(t)$; and (d) DC link voltage with proposed compensation.

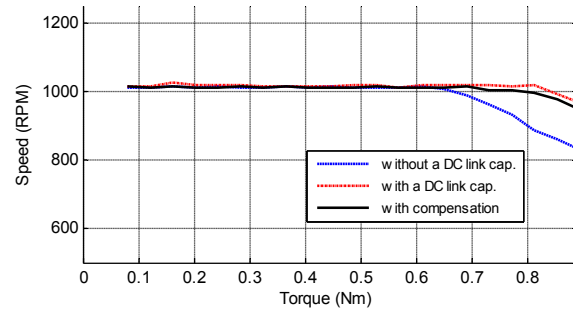


Fig. 15. Torque-speed curves without a DC link capacitor, with a 150 μF DC link capacitor and with proposed compensation for M1.

$$P_c = I^2 R_{ON} \quad (31)$$

By substitution, $P_c = 0.0098 \text{ W}$.

Turn on and turn off losses can be found by using the turn on and turn off switching energy parameters in the datasheet. The total switching energy is the sum of turn on and off energies. From the datasheet of the switch, the total switching energy (E_s) is found to be equal to 223 μJ . Switching loss (P_s) can be calculated by,

TABLE III
INPUT THD, TORQUE RIPPLE AND EFFICIENCY

| | Conventional converter with stiff DC link | Converter without compensation | Converter with compensation |
|---|---|--------------------------------|-----------------------------|
| THD of the input current | 203.4 % | 114.3 % | 105.6 % |
| Torque ripple due to the absence of the DC link capacitor | 0% | 100 % | 8 % |
| Efficiency of the converter | 82.3 % | 81.6 % | 81.4 % |

$$P_s = E_s f_s \quad (32)$$

where f_s is the switching frequency. For the additional switch, the switching frequency is 100 Hz for a 50Hz mains supply. Substituting to (32) yields $P_s = 0.023$ W. From (31) and (32) the total switching loss introduced by the compensation IGBT is found to be equal to 0.032W, which is negligible compared to the output power level of the motor drive.

Fig. 15 shows the torque-speed curves for M1. According to Fig. 15, the speed of M1 can be controlled until the current controller starts to limit the phase current. The maximum torque that can be delivered from the motor drive is lower without the DC link capacitor for a given value of peak current limit.

As evident from Fig. 15, the same amount of torque as a conventional BLDC motor drive can be obtained by using the proposed compensation. THD of the input current is measured with the DC link capacitor, without the DC link capacitor, and with proposed torque ripple compensation. The efficiency of the drive state is measured to investigate the effect of having additional compensation stage. Obtained results are tabulated in Table III. According to the results, a significant improvement in THD is evident with the proposed compensation technique in comparison to a conventional BLDC motor drive. Ideally, with the proposed compensation, the torque ripple due to the absence of the DC link capacitor is fully eliminated. However, due to the slower response time of the electronics, an 8% ripple in the torque was observed. Without the compensation capacitor, the torque ripple can be 100%. Commutation torque ripple is same despite the presence of the DC link capacitor or compensation stage. Hence, the commutation torque ripple is neglected. Due to the lower losses associated with the additional compensation stage, the efficiency of the converter is similar for all three configurations.

The slower response time and the ripples in the experimental current waveform are mainly due to the limitations of the microcontroller, the output drive stage and the current measurement technique. Nevertheless, the good agreement between the analytical results, simulated results and experimental results verifies the accuracy of the proposed model and the torque ripple compensation technique. The results produced by this analysis can be used to derive the parameters to design a low cost BLDC motor drive for a given specification with comparable performance.

VI. CONCLUSION

A simple mathematical model and a compensation technique for inherent torque ripples of a BLDC motor drive, operated without a DC link capacitor, have been proposed. The simplicity of the model permits the controller to be implemented on inexpensive microcontroller platforms with very low resources. With the proposed technique for compensating torque ripples, comparable performance to a conventional BLDC motor drive with a large DC link capacitor can be achieved. However, with the torque ripple compensation technique, the overall complexity of the motor drive has been increased, which is a major disadvantage. Based on the application, major augmentations in both hardware and firmware may be required. The good agreement between the theoretical results, simulated results and experimental results demonstrate the accuracy of the simple buck model and the effectiveness of the proposed compensation technique. The proposed compensation technique is expected to be useful for manufacturing low cost BLDC motor drives with comparable performance.

APPENDIX

PARAMETERS OF THE MOTORS

| Parameter | Motor M1 | Motor M2 |
|-----------------|-------------------------|-------------------------|
| R | 3 Ω | 7.5 Ω |
| $L - M$ | 15 mH | 54 mH |
| J | 0.0024 kgm ² | 0.0024 kgm ² |
| F | 0.001 Nms | 0.001 Nms |
| P | 3 | 3 |
| Back emf | Trapezoidal | Trapezoidal |
| Torque constant | 0.8 NmA ⁻¹ | 1.4 NmA ⁻¹ |
| Rated power | 250 W | 250 W |

REFERENCES

- [1] R. Krishnan, *Electric Motor Drives, Modeling, Analysis, and Control*. Prentice Hall, 2001.
- [2] R. Krishnan, *Permanent Magnet Synchronous and Brushless DC Motor Drives*. CRC Press, 2010.
- [3] J. F. Gieras, *Permanent Magnet Motor Technology - Design and Applications*: CRC Press, 2010.
- [4] V. Sankaran, F. Rees, and C. Avant, "Electrolytic capacitor life testing and prediction," in *Industry Applications Conference, 1997. Thirty-Second IAS Annual Meeting, IAS '97., Conference Record of the 1997 IEEE*, vol. 2, Oct. 1997, pp. 1058–1065.
- [5] H. K. Samitha Ransara and U. K. Madawala, "A Low Cost Brushless DC Motor Drive," in *6th IEEE Conference on Industrial Electronics and Applications, (IEEE ICIEA)*, Jun. 2011, pp. 2723–2728.
- [6] Zhu, Z., Wu, L. and Mohd Jamil, M., "Distortion of Back-EMF and Torque of PM Brushless Machines Due To Eccentricity," *IEEE Trans. on Magnetics*, no.99.
- [7] Carlson, R., Tavares, A.A., Bastos, J.P., Lajoie-Mazenc, Michel, "Torque ripple attenuation in permanent magnet synchronous motors," *Industry Applications Society Annual Meeting, 1989., Conference Record of the 1989 IEEE*, vol., no., pp.57–62 vol.1, Oct. 1989.
- [8] England, T.R., "Unique surface-wound brushless servo with improved torque ripple characteristics," *IEEE Trans on Ind. Applications*, vol.24, no.6, pp.972–977, Nov/Dec 1988.

- [9] Dae-kyong Kim, Kwang-Woon Lee, Byung-Ii Kwon, "Commutation Torque Ripple Reduction in a Position Sensorless Brushless DC Motor Drive," *IEEE Trans. on Power Electron.*, vol.21, no.6, pp.1762-1768, Nov. 2006.
- [10] Mohamed, Y. A -R I; El-Saadany, E.F., "A Current Control Scheme with an Adaptive Internal Model for Robust Current Regulation and Torque Ripple Minimization in PMSM Vector Drive," *Electric Machines & Drives Conference, 2007. IEMDC '07. IEEE International*, vol.1, pp.300-305, May 2007.
- [11] Tewari, S.V., Indu Rani, B., "Torque Ripple Minimization of BLDC Motor with Un-Ideal Back EMF," *Emerging Trends in Engineering and Technology (ICETET), 2009 2nd International Conference on*, vol., no., pp.687-690, Dec. 2009.
- [12] Haifeng Lu Zhang, Lei Wenlong Qu, "A New Torque Control Method for Torque Ripple Minimization of BLDC Motors With Un-Ideal Back EMF," *IEEE Trans. on Power Electron.*, vol.23, no.2, pp.950-958, Mar. 2008.
- [13] Ki-Yong Nam, Woo-Taik Lee, Choon-Man Lee, Jung-Pyo Hong, "Reducing torque ripple of brushless DC motor by varying input voltage," *IEEE Trans. on Magnetics*, vol.42, no.4, pp.1307-1310, Apr. 2006.
- [14] Berendsen, C.-S, Champenois, G., Bolopion, A., "Commutation strategies for brushless DC motors: influence on instant torque," *IEEE Trans. on Power Electron.*, vol.8, no.2, pp.231-236, Apr. 1993.
- [15] Ozturk, S.B., Alexander, W.C., Toliyat, H.A., "Direct Torque Control of Four-Switch Brushless DC Motor With Non-Sinusoidal Back EMF," *IEEE Trans. on Power Electron.*, vol.25, no.2, pp.263-271, Feb. 2010.
- [16] Yongchang Zhang, Jianguo Zhu, Wei Xu, Youguang Guo, "A Simple Method to Reduce Torque Ripple in Direct Torque-Controlled Permanent-Magnet Synchronous Motor by Using Vectors With Variable Amplitude and Angle," *IEEE Trans. on Ind. Electron.*, vol.58, no.7, pp.2848-2859, July 2011.
- [17] Yanhui Xu, Parspour, N., Vollmer, U., "Torque Ripple Minimization Using Online Estimation of the Stator Resistances With Consideration of Magnetic Saturation," *IEEE Trans. on Ind. Electron.*, vol.61, no.9, pp.5105-5114, Sept. 2014.
- [18] Jiancheng Fang, Haitao Li and Bangcheng Han, "Torque Ripple Reduction in BLDC Torque Motor With Nonideal Back EMF," *IEEE Trans. on Power Electron.*, vol.27, no.11, pp.4630-4637, Nov. 2012.
- [19] Fang, J., Zhou, X., and Liu, G. , "Instantaneous Torque Control of Small Inductance Brushless DC Motor," *IEEE Trans. on Power Electron.*, vol.27, no.12, pp.4952-4964, Dec. 2012.
- [20] Fang, J., Zhou, X. and Liu, G., "Precise Accelerated Torque Control for Small Inductance Brushless DC Motor," *IEEE Trans. on Power Electron.*, vol.28, no.3, pp.1400-1412, March 2013.
- [21] Y. Ohnuma and J. Itoh, "Space vector modulation for a single phase to three phase converter using an active buffer," in *Power Electronics Conference (IPEC), 2010 International*, 2010, pp. 574-580.
- [22] Y. Ohnuma and J. I. Itoh, "Novel control strategy for single-phase to three-phase power converter using an active buffer," in *Power Electronics and Applications, 2009. EPE '09. 13th European Conference on*, pp. 1-10.
- [23] H. K. Samitha Ransara and U. K. Madawala, "A technique for torque ripple compensation of a low cost BLDC motor drive," in *IEEE International Conference on Industrial Technology (ICIT 2013)*, Feb. 2013, pp. 222-227.
- [24] H. K. Samitha Ransara and U. K. Madawala, "Modelling and Analysis of a Low Cost BLDC Motor," in *IEEE International Conference on Industrial Technology (ICIT 2013)*, Feb. 2013, pp. 356-36



H. K. Samitha Ransara received the B.Sc. Eng. (Hons) degree in electrical engineering with a first class pass from University of Moratuwa, Sri Lanka in 2008 and the Ph.D. degree in power electronics from The University of Auckland, New Zealand, in 2015. Since 2012, he is working as an electronics and embedded software engineer in Wellington Drive Technologies, New Zealand in the areas of motor control and power electronic converters. His main research areas include state observer based sensorless permanent magnet synchronous motor control and power electronic converters that are suitable for consumer electronics and green energy applications.



Udaya K. Madawala (M'93-SM'06) received the B.Sc.(Hons.) degree in electrical engineering from the University of Moratuwa, Moratuwa, Sri Lanka, in 1987 and the Ph.D. degree in power electronics from The University of Auckland, Auckland, New Zealand, in 1993. Since 1997, after working in industry, he has been with the Department of Electrical and Computer Engineering, The University of Auckland, where he is currently a Professor. He is a Consultant to industry.

His research interests include the fields of power electronics, inductive power transfer, and renewable energy. Dr. Madawala is an active IEEE volunteer and serves as an Associate Editor for both the IEEE TRANSACTIONS ON INDUSTRIAL ELECTRONICS and the IEEE TRANSACTIONS ON POWER ELECTRONICS. He is a member of the Power Electronics Technical Committee and also the Chairman of the Joint Chapter of IEEE Industrial Electronics Society and IEEE Industrial Applications Society in New Zealand (north).